JOURNAL OF MATERIALS SCIENCE 29 (1994) 2053–2062

Elastic–plastic thermal stresses and deformation of short-fibre composites

M. L. DUNN, M. TAYA
Department of Mechanical Engineering, University of Washington, Seattle, Washington 98195, USA

A micromechanics model is proposed to analyse residual stresses and deformations that develop in short-fibre composites upon an applied uniform temperature change. The model is based on Eshelby's equivalent inclusion method and treats the interaction among fibres at finite volume fractions through the Mori–Tanaka mean field theory. The model treats the matrix as an elastic/plastic material while the fibre is elastic and is able to account for the effects of the composite microgeometry. To this end, the effects of misoriented short fibres, the orientation of which is described by a density distribution function, are considered. Numerical results obtained from the proposed model indicate that the misorientation of short fibres has a significant effect on both the stress and deformation behaviour of short-fibre composites.

1. Introduction

The thermoelastic/inelastic behaviour of short-fibre composites is of considerable interest in the assessment of these materials as candidates for high-temperature structural applications such as jet-engine turbine components. For high-temperature applications, both the stress and deformation of a short-fibre composite are of importance. A primary factor contributing to the stress and deformation is the composite microgeometry, which in turn is greatly affected by processing techniques. Fibres, intended to be aligned, will in general become misoriented during processing, and the amount of fibre misorientation is generally a function of the processing technique. The purpose of this work is to investigate the effect of microgeometry on the thermal stress and deformation of a short-fibre composite. To this end, a micromechanics model is developed to predict the stress and deformation of a short-fibre composite subjected to an applied uniform thermal load.

This investigation of the effects of the microgeometry on the stress and deformation behavior of a short-fibre composite is motivated in part by the belief that advances in image processing and analysis techniques will soon make possible the rapid and accurate characterization of the three dimensional microgeometry of a short-fibre composite. With the knowledge of the effects of the microgeometry on the thermomechanical performance of a short-fibre composite, such characterization could be readily applied as a quality control measure in a production environment.

With regard to the microgeometry, this work considers two important aspects: the shape and misorientation of short fibres. The analytical model is developed within the framework of the equivalent inclusion idea of Eshelby [1] and accounts for the interaction among misoriented short fibres through the mean-field theory of Mori & Tanaka [2]. The general applicability of the proposed model is demonstrated, as it is applied to determine thermal residual stresses and thermal expansion coefficients in the elastic and elastic–plastic regimes.

The modelling of elastic thermal residual stresses and thermal expansion coefficients (CTEs) of composite materials has received considerable attention in the literature. The key works with regard to thermal expansion of composite materials are those of Levin [3] and Rosen & Hashin [4], who derived exact connections between the effective thermal expansion coefficients and elastic moduli of elastic composite materials. The analysis of particular composite microstructures, however, is primarily devoted to simpler microstructural geometries. For example, spherical particulate [5–7] and aligned continuous fibre [8,9] reinforced composites have received extensive research. Eshelby's equivalent inclusion method has been applied to model short-fibre composites containing aligned spheroidal fibres [10–12]. The effect of misoriented short fibres in a composite has also been analysed with regard to thermal stresses [13] and elastic CTE [14,15].

With regard to the elastic–plastic behaviour, many analyses have been directed toward composites under the influence of applied mechanical and thermal loads, to predict properties such as yield strength, work hardening rate, thermal expansions, and the flow behaviour of short-fibre composites [16–18]. Hysteresis experienced upon cyclic thermal loading has been considered by Wakashima *et al.* [19] who modelled the elastic–plastic deformations of composites reinforced by aligned thin discs or continuous fibres.

In this work, fundamental ideas regarding misoriented short-fibre composites that are utilized

0022–2461

routinely in this work are presented in Section 2. In Section 3, approximate expressions for the thermal residual stresses in a misoriented short-fibre composite are obtained for both an elastic and elastic–plastic deforming matrix. The thermal expansion coefficients of the same misoriented short-fibre composite in both the elastic and elastic–plastic regimes are presented in Section 4. The analysis is strictly valid only for monotonic loading, but can be applied in an incremental manner to general loading. The utility of the proposed model is exhibited in Section 5 as numerical results are presented for some metal matrix composites of practical interest. Finally concluding remarks are made in Section 6.

2. Misoriented short-fibre composites

In the following analysis, the residual stress and deformation of a misoriented short-fibre composite (MSFC) will be obtained. It is thus desirable to briefly review some general concepts regarding the orientation of fibres in a composite and the application of these concepts to MSFCs. It is first noted that the term misoriented may be misleading, in that it implies that the fibres in a composite should be oriented in some prescribed manner, but are not. A MSFC may well contain misoriented fibres due to imperfections in processing techniques; however, the existence of misoriented fibres may be by design, i.e. to improve the composite properties in preferred directions.

In the analysis of a MSFC it is necessary to consider the auxiliary problem of an infinite matrix in which a short fibre is embedded at some general orientation (Fig. 1). The subsequent analysis is most easily facilitated by defining two coordinate systems; a local coordinate system (x'_1, x'_2, x'_3) in which the x'_3 axis coincides with the axis of a representative fibre and a global coordinate system (x_1, x_2, x_3). The local and global coordinate systems are related by the transformation:

$$x = \boldsymbol{Y} \cdot x' \quad x' = \boldsymbol{Y}^{-1} \cdot x \tag{2.1}$$

where $\boldsymbol{Y}$ is a second-order tensor, the components of which are functions of the spherical polar angles θ and φ. It will be necessary to determine the average of a second-order tensor (typically the stress and strain) over the domain consisting of all fibres. The determination of this quantity is two-fold and consists of (a) the computation of the orientation dependent average strain in a single fibre, and (b) the subsequent average of this quantity over all possible fibre orientations. The distribution of possible fibre orientations is defined by the use of a density distribution function, $\rho(\theta, \varphi)$ where θ and φ are the angles of a spherical polar coordinate system. Physically, the distribution function, $\rho(\theta, \varphi)$, is a description of the number of fibres intersecting the surface of a unit sphere.

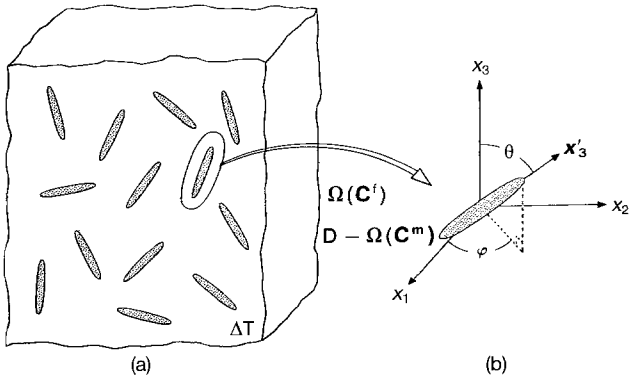

Figure 1 Misoriented short-fibre composite system. (a) Domain of the analytical model, (b) definition of the coordinate system used.

In this work, two modes of fibres misorientation will be considered; two-dimensional in-plane, and three-dimensional axisymmetric. These are applicable to composites produced by compression moulding and extrusion, and allow the simulation of composites containing fibres randomly distributed 'in-plane' but misoriented in the 'thickness' direction. For 2-D in-plane misorientation, all fibres are confined to the x_2–x_3 plane, and for 3-D axisymmetric misorientation all fibres are uniformly distributed over the 2π range of φ. Thus for each of these two modes of misorientation, $\rho(\theta, \varphi)$ is reduced to a function of θ only. For each mode of misorientation, two distribution functions are considered: uniform, $\rho(\theta) = \rho_0$ and cosine-type, $\rho(\theta) = \rho_0 \cos(a\theta)$. The cosine-type distribution is used to simulate a normal distribution while allowing the closed form integration over the finite range of the distribution. Each distribution function is assumed to be bounded by the cut-off angle, $\pm \beta$, such that all fibres lie in the range $-\beta \leqslant \theta \leqslant +\beta$. Due to the normalization requirement of $\rho(\theta)$, ρ_0 and a are functions of the cut-off angle alone [13].

The principle use of the distribution functions is to perform the weighted integration (or averaging) of a quantity $\boldsymbol{F}(\theta, \varphi)$ over the domain of all fibres. To this end, $\boldsymbol{F}(\theta, \varphi)$ is first integrated over the domain of a single fibre, the result of which is orientation-dependent. This orientation-dependent quantity is then integrated (averaged) over all possible fibre orientations. In particular, the following relation will frequently be used:

$$\frac{1}{V_D}\int_\Omega \boldsymbol{F}(\theta, \varphi)\, dV = f \frac{\int_0^{2\pi}\int_0^{\pi/2} \langle \boldsymbol{F}(\theta, \varphi)\rangle \rho(\theta) \sin\theta\, d\theta\, d\phi}{\int_0^{2\pi}\int_0^{\pi/2} \rho(\theta) \sin\theta\, d\theta\, d\phi} \tag{2.2}$$

where the integral over Ω is over the domain consisting of all fibres and the volume of the composite, V_D, has been defined by:

$$f = \frac{V_\Omega}{V_D} = \frac{\int_0^{2\pi}\int_0^{\pi/2} \rho(\theta)\, V \sin\theta\, d\theta\, d\phi}{V_D} \tag{2.3}$$

In Equation 2.3, V is the volume of a single fibre, V_Ω is the volume of the domain of all fibres, f is the volume fraction of fibres, and $\langle \boldsymbol{F}(\theta, \varphi)\rangle$ is the volume average of $\boldsymbol{F}(\theta, \varphi)$ over a single fibre. In the following analysis, quantities similar to the left hand side of Equation 2.2 will routinely be evaluated in this manner.

3. Thermal residual stresses

3.1. Elastic analysis

The domain of the analytical model consists of an infinite elastic body containing misoriented short fibres, as shown in Fig. 1a. The domains of the entire composite and of the fibres are denoted by D and Ω, respectively. The domain of the matrix is thus denoted by D–Ω. The stiffness tensors of the matrix and fibre are C_m and C_f, respectively. The fibres are modelled as ellipsoidal inhomogeneities (prolate spheroids) of the same size. For simplicity, in the results that are presented both the fibres and the matrix are assumed to be isotropic. The model, however can easily accommodate the case of a composite with anisotropic fibres [15, 20] and in principle can accommodate an anisotropic matrix; however, except for transversely isotropic matrix materials, the computations for the case of an anisotropic matrix become quite rigorous [21]. At this point it is also assumed that the fibres and matrix deform elastically, and that the fibre–matrix interface is perfectly bonded. Later these requirements will be relaxed to allow for elastic–plastic deformations of the matrix material.

Consider the composite system containing misoriented short fibres as shown in Fig. 1a. The local coordinates associated with a representative fibre are x'_1, x'_2 and x'_3 where x'_3 coincides with the fibre axis as shown in Fig. 1b. The global coordinates are x_1, x_2, and x_3. Now consider that this composite system is subjected to a uniform temperature change ΔT. The temperature change induces a thermal stress field in the composite due to the mismatch in coefficients of thermal expansion (CTEs) between the matrix and fibres. The temperature change is assumed to be uniform, thus no thermal stresses are developed due to temperature gradients within the composite. The thermal stress field in the matrix, however, is non-uniform due to disturbances by all of the fibres in the composite.

When averaged over the matrix domain, the thermal stress can be related to the volume averaged strain in the matrix $\bar{e}$ by:

$$\langle \boldsymbol{\sigma} \rangle_m = C_m \cdot \bar{e} \tag{3.1}$$

where bold characters denote tensorial quantities, and a dot denotes the inner product between two tensors. If a single fibre is introduced into the composite system with an orientation as shown in Fig. 1b, the stress in the fibre (in local coordinates) can be determined by the use of Eshelby's equivalent inclusion method [1, 2, 10, 22] in which the inhomogeneity (Ω) with thermal strain $e^{T'}$ is replaced with an equivalent inclusion (Ω) with a fictitious eigenstrain $e^{*E'}$ to yield:

$$\boldsymbol{\sigma} = C_f \cdot (\bar{e}' + e' - e^{T'}) = C_m \cdot (\bar{e}' + e' - e^{*E'}) \tag{3.2}$$

In Equation 3.2, e' is the local disturbance strain due to the introduction of the single fibre and $\bar{e}'$ is the volume averaged strain defined by Equation 3.1, but expressed in the local coordinates. The thermal strain, $e^{T'}$ is developed due to the mismatch between CTE tensors of the matrix (α_m) and fibre (α_f) under a uniform temperature change, $\Delta T = T_L - T_H$ and is given by $e^{T'} = (\alpha_f - \alpha_m)\Delta T = \alpha \Delta T$ where an isotropic CTE is now assumed to simplify computations. In the following it is assumed that the temperature change is a decrease, thus T_H is the initial high temperature (e.g. a processing temperature) and T_L is the final low temperature (e.g. room temperature). Following Eshelby [1], e' is related to $e^{*E'}$ by:

$$e' = S \cdot e^{*E'} \tag{3.3}$$

where S is Eshelby's tensor and is a function of the fibre geometry (aspect ratio) and Poisson's ratio of the matrix (ν_m) and is tabulated elsewhere [10, 22].

Substitution of Equation 3.3 into Equation 3.2, followed by some algebraic manipulation, yields the quantity:

$$e' - e^{*E'} = (S - I) \cdot [(C_f - C_m) \cdot S + C_m]^{-1} \cdot [-(C_f - C_m) \cdot \bar{e}' + C_f \cdot e^{T'}] \tag{3.4}$$

where I is the 6×6 identity matrix. As the added single fibre can be regarded as any fibre in the composite, Equations 3.2 and 3.4 hold for any inclusion in the matrix. It should be noted that Equation 3.2 can also be written in terms of global coordinates.

Since $\boldsymbol{\sigma}$ in Equation 3.2 is induced internally in Ω, the volume average of $\boldsymbol{\sigma}$ over the entire composite domain must vanish. This requirement yields:

$$\bar{e} + \frac{1}{V_D} \int_\Omega (e - e^{*E}) \, dV = 0 \tag{3.5}$$

where V_D is the volume of the entire composite (D). Once $\bar{e}$ is computed from Equation 3.5, the average stress in the matrix, $\langle \boldsymbol{\sigma} \rangle_m$, can be computed from Equation 3.1. To solve for $\bar{e}$, the quantity $(e' - e^{*E'})$ of Equation 3.4 must be transformed to global coordinates. The transformation from local to global coordinates is accomplished by use of the transformation matrices for second-order tensors, Z and $X = Z^{-1}$ where Z relates the quantity $(e - e^{*E})$ in global coordinates to that in local coordinates, i.e. $e - e^{*E} = Z \cdot (e' - e^{*E'})$. The components of the transformation matrices, Z and X, are dependent on the assumed type of misorientation and thus they are functions of the spherical polar angles φ and θ. The transformation of Equation 3.4 to global coordinates yields:

$$e - e^{*E} = Z \cdot A \cdot X \cdot \bar{e} + Z \cdot B \tag{3.6}$$

where:

$$A = -(S - I) \cdot [(C_f - C_m) \cdot S + C_m]^{-1} \cdot (C_f - C_m)$$
$$B = (S - I) \cdot [(C_f - C_m) \cdot S + C_m]^{-1} \cdot C_f \cdot e^{T'} \tag{3.7}$$

Equation 3.7 is substituted into Equation 3.5 and the volume integral in Equation 3.5 is then evaluated by the use of the density distribution functions of fibre orientation as illustrated by Equation 2.2. Upon substitution of Equation 3.6 into 3.5 and evaluation of the volume integral, the subsequent equation can be solved for $\bar{e}$ to yield:

$$\bar{e} = -\frac{f}{\psi^i} \left[I + \frac{f}{\psi^i} P \right]^{-1} \cdot Q \cdot B \tag{3.8}$$

where f is the volume fraction of fibres, P and Q are

6×6 matrices dependent on the distribution function of fibre orientation, $\rho(\theta, \varphi)$, and ψ^i is a function of the fibre orientation distribution. The quantity ψ^i and the matrices $\boldsymbol{P}$ and $\boldsymbol{Q}$ are given explicitly in the Appendix.

Once $\bar{e}$ is determined from Equation 3.8, e^{*E} is readily evaluated from Equation 3.6 and the volume averaged thermal stress in the matrix $\langle\sigma\rangle_m$ is calculated from Equation 3.1. The average thermal stress in the fibre, $\langle\sigma\rangle_f$, is then determined from the requirement of self-equilibrium of the thermal stresses:

$$f\langle\sigma\rangle_f = -(1-f)\langle\sigma\rangle_m \tag{3.9}$$

For use in future computations it is convenient to rewrite the average stress in the matrix, Equation 3.1, in terms of the thermal mismatch strain $e^{T'}$:

$$\langle\sigma\rangle_m = \boldsymbol{L}\cdot e^{T'} \tag{3.10}$$

where:

$$\boldsymbol{L} = -\frac{f}{\psi^i}\left\{\boldsymbol{C}_m\cdot\left[\boldsymbol{I}+\frac{f}{\psi^i}\boldsymbol{P}\right]^{-1}\cdot\boldsymbol{Q}\cdot\boldsymbol{K}\right\}$$

$$\boldsymbol{K} = (\boldsymbol{S}-\boldsymbol{I})\cdot[\boldsymbol{C}_f-\boldsymbol{C}_m)\cdot\boldsymbol{S}+\boldsymbol{C}_m]^{-1}\cdot\boldsymbol{C}_f \tag{3.11}$$

It is also convenient to express the explicit components of $\langle\sigma\rangle_m$ of Equation 3.10 in terms of $\alpha\Delta T$:

$$\langle\sigma_{ij}\rangle_m = L_i\alpha\Delta T \quad \text{for } i=j$$

$$\langle\sigma_{ij}\rangle_m = 0 \quad \text{for } i\neq j \tag{3.12}$$

where:

$$L_i = L_{i1}+L_{i2}+L_{i3} \tag{3.13}$$

and L_{ij} are the components of $\boldsymbol{L}$ as defined by Equation 3.11.

3.2. Onset of yield in the matrix

At this point the assumption of a completely elastic matrix is relaxed, and it is assumed that the matrix is able to undergo elastic–plastic deformations. It is also assumed that between T_H and T_L there is a temperature, T_{YL}, such that the thermal stresses that are developed upon cooling from T_H to T_{YL} are large enough to initiate uniform yielding of the matrix material. Yielding of the matrix material thus begins at T_{YL} and the temperature drop from T_{YL} to T_L causes further plastic deformations [19, 23].

If the matrix is to begin yielding at T_{YL}, then the average matrix stresses, $\langle\sigma\rangle_m$, must satisfy a yield criterion. Here the von Mises yield criterion is assumed and can be expressed as:

$$[\langle\sigma_{11}\rangle_m-\langle\sigma_{22}\rangle_m]^2+[\langle\sigma_{22}\rangle_m-\langle\sigma_{33}\rangle_m]^2 + [\langle\sigma_{33}\rangle_m-\langle\sigma_{11}\rangle_m]^2 = 2\sigma_{YL}^2 \tag{3.14}$$

where σ_{YL} is the matrix yield stress (at T_L) in simple tension. The onset of yield is then determined by substitution of Equations 3.12 into Equation 3.14 which, after some manipulation, yields:

$$\alpha\Delta T_{L_{cr}} = \frac{\sqrt{2}\sigma_{YL}}{[(L_1-L_2)^2+(L_2-L_3)^2+(L_3-L_1)^2]^{1/2}} \tag{3.15}$$

where $\alpha\Delta T_{L_{cr}}$ defines the normalized critical temperature change required to initiate yielding of the matrix material upon cooling, i.e. $\Delta T_{L_{cr}} = T_{YL} - T_H$. In other words, for all $\Delta T < \Delta T_{L_{cr}}$, all deformations will be elastic.

3.3. Further plastic deformations

If $\Delta T > \Delta T_{L_{cr}}$, the large elastic stresses that would otherwise exist in the matrix will relax due to plastic deformations. To compute the plastic deformations, it is assumed that the temperature drop from T_H to T_L induces a uniform plastic strain e^{PL} in the matrix, and that the matrix is a non-hardening material. The simplifying assumption of a uniform plastic strain in the matrix neglects the effects of microyielding that is known to occur near the fibre–matrix interface upon relatively low temperature changes. As has been pointed out by Withers *et al.* [24] and Warner & Stobbs [25], however, it is average stress field in the matrix that is believed to control the macroscopic response of the composite. For macroscopic plastic deformations to occur, dislocations must move large distances through the composite relative to the typical spacing of fibres. The local stress fields near the fibres (which are responsible for the localized microyielding) do not contribute to macroscopic deformations of the composite as they do not encourage the movement of the dislocations over substantial distances. To account for the effects of localized plastic flow, a more rigorous approach is required, such as consideration of the effects of dislocations punched out from the fibre–matrix interface.

The uniform plastic strain, e^{PL}, is assumed to satisfy the incompressibility requirement $e_{ii}^{PL} = 0$. The stress due to this uniform plastic strain (which is presently unknown) can be computed by use of Eshelby's equivalent inclusion method. This solution procedure is shown schematically in Fig. 2. The stress field in the composite system in Fig. 2 can be determined by the straightforward application of Eshelby's equivalent inclusion method (as with the inelastic thermal strain in Section 3.1) to yield:

$$\sigma' = \boldsymbol{C}_f\cdot(\bar{e}'+e'+e^{PL'}) = \boldsymbol{C}_m\cdot(\bar{e}'+e'-e^{*P'}) \tag{3.16}$$

where the form of e^{PL} is assumed to be (in local coordinates):

$$e^{PL'} = \left[-\frac{\varepsilon^{PL}}{2}, -\frac{\varepsilon^{PL}}{2}, \varepsilon^{PL}, 0, 0, 0\right]^T \tag{3.17}$$

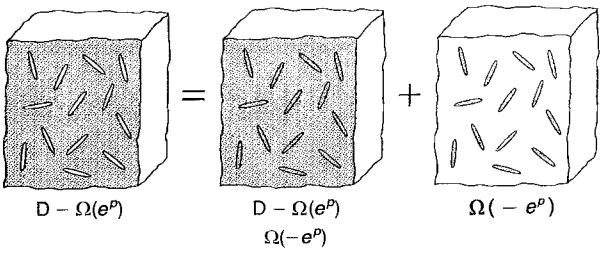

Figure 2 Schematic representation of the calculation of the uniform plastic strain in the matrix and the corresponding overall strain of the composite.

Thus the form of e^{PL} is a result of the averaging over all possible fibre orientations. Equation 3.16 is mathematically equivalent to Equation 3.2, with the exception that $e^{T'}$ has been replaced with $-e^{PL'}$. Thus, using Equation 3.10, the solution for the resulting stress field can be immediately written as:

$$\langle \boldsymbol{\sigma} \rangle_m^{PL} = -\boldsymbol{L} \cdot e^{PL'} \tag{3.18}$$

where $\langle \boldsymbol{\sigma} \rangle_m^{PL}$ is the average stress in the matrix due to the uniform plastic strain at the low temperature, $e^{PL'}$. As in Equation 3.10, the stress components can be written explicitly as:

$$\begin{aligned} \langle \sigma_{ij} \rangle_m^{PL} &= L_i^* \varepsilon^{PL} \quad \text{for } i = j \\ \langle \sigma_{ij} \rangle_m^{PL} &= 0 \quad \text{for } i \neq j \end{aligned} \tag{3.19}$$

where:

$$L_i^* = \frac{L_{i1}}{2} + \frac{L_{i2}}{2} - L_{i3} \tag{3.20}$$

It is reiterated that ε^{PL} is still an unknown and the stress field of Equation 3.19 has simply been expressed as a function of the unknown plastic strain, ε^{PL}.

The plastic strain, ε^{PL}, can be determined by following either of two approaches: an energy or a stress approach, both of which have been shown to be equivalent [26]. In this work the stress approach is used. Following the stress approach, the yield criterion of Equation 3.14 is applied to the unknown total stress existing at $T_L(\langle \underset{\sim}{\sigma} \rangle_m^T = \langle \underset{\sim}{\sigma} \rangle_m + \langle \underset{\sim}{\sigma} \rangle_m^{PL})$ to yield a quadratic equation in ε^{PL} which is easily solved to yield:

$$\varepsilon^{PL} = \frac{-B \pm (B^2 - 4AC)^{1/2}}{2A} \tag{3.21}$$

In Equation 3.21 the (+) and (−) roots are used for compressive and tensile yielding, respectively, and the constants A, B and C are functions of the material properties of the constituents, the geometry of the misoriented short-fibre composite, the temperature change (ΔT), and the matrix yield strength (σ_{YL}) and are given by:

$$\begin{aligned} A &= R_1^{*2} + R_2^{*2} + R_3^{*2} \\ B &= 2\alpha\Delta T[R_1 R_1^* + R_2 R_2^* + R_3 R_3^*] \\ C &= [R_1^2 + R_2^2 + R_3^2]\alpha^2 \Delta T^2 - 2\sigma_{YL}^2 \end{aligned} \tag{3.22}$$

where:

$$\begin{aligned} R_1 &= L_1 - L_2 \quad & R_1^* &= L_1^* - L_2^* \\ R_2 &= L_2 - L_3 \quad & R_2^* &= L_2^* - L_3^* \\ R_3 &= L_3 - L_1 \quad & R_3^* &= L_3^* - L_1^* \end{aligned} \tag{3.23}$$

For the case of a transversely isotropic composite (a 3-D axisymmetric MSFC or a 2-D in-plane random MSFC), Equation 3.21 reduces to:

$$\varepsilon^{PL} = \frac{\sigma_{YL} - (L_3 - L_1)\alpha\Delta T}{L_3^* - L_1^*} \tag{3.24}$$

Equation 3.24, however, does not imply that the plastic strain is the same for the 3-D axisymmetric and 2-D in-plane random MSFCs as the values of L_i and L_i^* (which are functions of the material properties and the geometry of the composite) will differ in each case.

With the plastic strain, ε^{PL} (thus e^{PL}) known, the residual stresses in the matrix at T_L are given by the sum of Equations 3.12 and 3.19. The average stresses in the fibre can then be found from the requirement of self equilibrium, Equation 3.9.

4. Deformation of short-fibre composites

Thus far a general model has been developed to predict the thermal stress state in a two-phase misoriented short-fibre composite where the matrix is assumed to undergo elastic–plastic deformations. The immediate application of the present model is to the thermal residual stress that is developed in a composite, upon cooling from a high processing temperature to room temperature. In the subsequent sections, the proposed model is extended/applied to model the deformation of MSFCs under uniform temperature changes. Of particular engineering interest are the coefficients of thermal expansion in the elastic and elastic–plastic regimes.

4.1. Coefficients of thermal expansion

The model that has been developed is now used to determine the coefficients of thermal expansion (CTEs) in the elastic and elastic–plastic regimes of a MSFC. It is noted that the results obtained for the elastic CTE have been previously obtained by Takao [14] but are included within the framework of the present model for completeness.

The effective CTE of a composite, α_e, is defined as:

$$\alpha_e = \frac{\gamma_D}{\Delta T} = \frac{1}{\Delta T}\frac{1}{V_D}\int_D e^{total}\, dV \tag{4.1}$$

where γ_D is the average macroscopic strain in the composite, e^{total} is the total strain, and it is assumed that no initial strain exists. In the elastic case, after use of Equations 3.4 and 3.8 and some manipulation, γ_D^E (the average macroscopic elastic strain) can be expressed as:

$$\gamma_D^E = \frac{1}{V_D}\int_\Omega e^{*E}\, dV + \alpha_m \Delta T \tag{4.2}$$

In Equation 4.2 $e^{*E} = \boldsymbol{Z} \cdot e^{*E'}$ and is obtained by solving for $e^{*E'}$ from Equations 3.4 and 3.8 and then transforming the result to global coordinates. The integral in Equation 4.2 is then evaluated in the same manner as that in 3.5. The composite elastic CTE is then obtained upon substitution of Equation 4.2 into 4.1. For the case of an aligned short-fibre composite, Equation 4.2 can be expressed as:

$$\gamma_D^E = f e^{*E} + \alpha_m \Delta T \tag{4.3}$$

which agrees with the result obtained by Takao & Taya [15].

After the matrix yields, Equation 4.1 can still be used to compute the composite CTE; however the average macroscopic strain in the elastic-plastic regime, γ_D, is different as the total strain changes due to

the plastic relaxation. Following reasoning similar to that used to find γ_D^E, the macroscopic strain due to uniform plastic deformations, γ_D^p, is obtained as:

$$\gamma_D^p = \frac{1}{V_D}\int e^{*P}\,dV + e^{PL} \tag{4.4}$$

The quantity e^{PL} in Equation 4.4 is the average uniform plastic strain in the matrix, and is obtained by transforming $e^{PL'}$ to global coordinates and then averaging over all possible fibre orientations to yield:

$$e^{PL} = -\frac{1}{\psi^i}\cdot Q\cdot e^{PL'} \tag{4.5}$$

where ψ^i and Q are given in Appendix A. Substitution of Equations 4.4 and 4.5, and the temperature change in the elastic–plastic regime ($\Delta T - \Delta T_{cr}$) into Equation 4.1, yields the composite thermal expansion due to plastic deformations.

5. Results and discussion

In this section, numerical results obtained from the proposed model are presented for typical metal matrix composites of engineering interest. Material properties used in all computations are shown in Table I

TABLE I Material properties of composite constituents used in calculations

	E (GPa)	ν	CTE ($\times 10^{-6}\,°C^{-1}$)	σ_{YL}/T_L (MPa)/(°C)
Matrix materials				
2124 Al	67.6	0.33	24.7	50.8/20
Cu	124.0	0.34	17.6	39.2/20
Fibre materials				
SiC	427.1	0.17	4.3	—
Tungsten	358.0	0.285	4.75	—

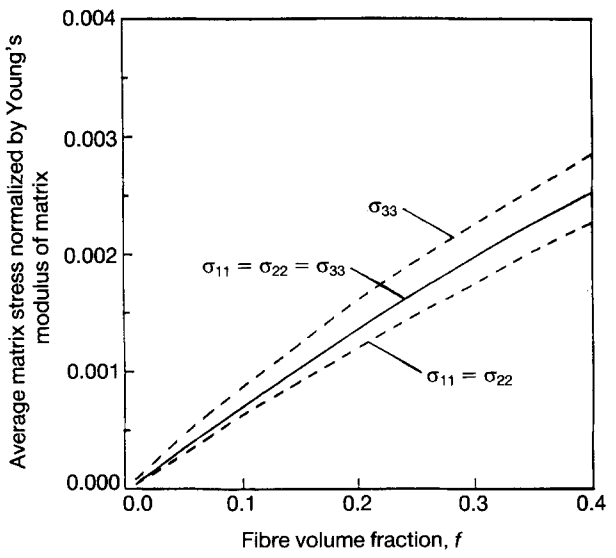

Figure 3 Variation of the normalized thermal residual stress in the matrix with the fibre volume fraction for 3-D axisymmetric misorientation with an elastic matrix. ——, uniform; ---, cosine-type distribution. $\alpha = 5$; $\beta = \pi/2$.

[19,23]. The computations in Figs 3–6 are for a short-fibre composite with 3-D axisymmetric misorientation, while those in Figs 7–11 are for one with 2-D inplane misorientation.

Figs 3 and 4 illustrate the effect of fibre volume fraction on the thermal residual stress state for a given set of geometric parameters and a temperature change of $\Delta T = -200\,°C$. Both Figs 3 and 4 show the relationship of the average matrix stresses normalized by Young's modulus of the matrix, $\langle\sigma\rangle_m/E_m$, for a given aspect ratio and cut-off angle. In Fig. 3, the cut-off angle is set at $\pi/2$, while in Fig. 4, it is set to $\pi/3$. The aspect ratio, α, is set to $\alpha = 5$ for both figures. In each figure, two types of distribution functions are investigated, uniform (solid lines) and cosine type (dashed lines). In the following discussion, the superscripts u and c denote stress components based on uniform

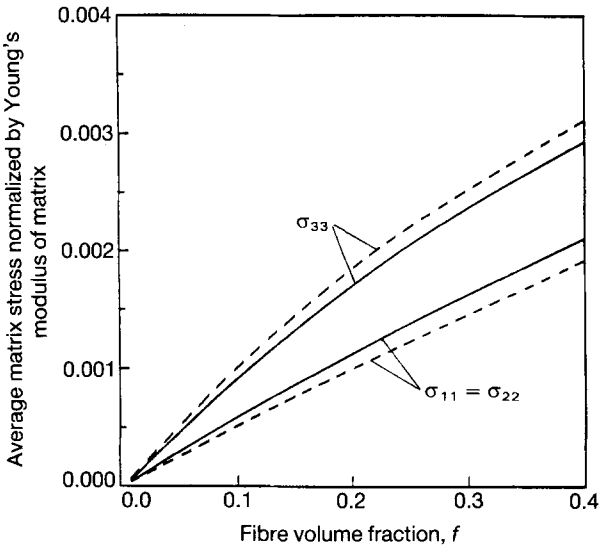

Figure 4 Variation of the normalized thermal residual stress in the matrix with the fibre volume fraction for 3-D axisymmetric misorientation with an elastic matrix. ——, uniform; ---, cosine-type distribution. $\alpha = 5$; $\beta = \pi/3$.

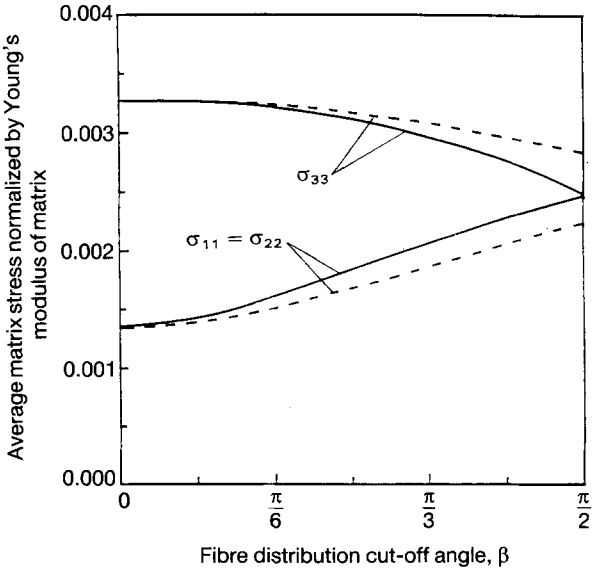

Figure 5 Variation of the normalized thermal residual stress in the matrix with the distribution cut-off angle for 3-D axisymmetric misorientation with an elastic matrix. ——, uniform; ---, cosine-type distribution. $\alpha = 5$; $f = 0.4$.

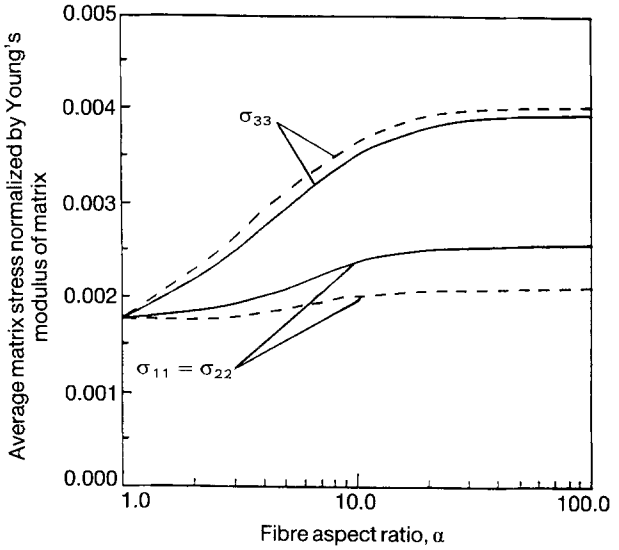

Figure 6 Variation of the normalized thermal residual stress in the matrix with the fibre aspect ratio for 3-D axisymmetric misorientation with an elastic matrix. ——, uniform; ---, cosine-type distribution. $\beta = \pi/3$; $f = 0.4$.

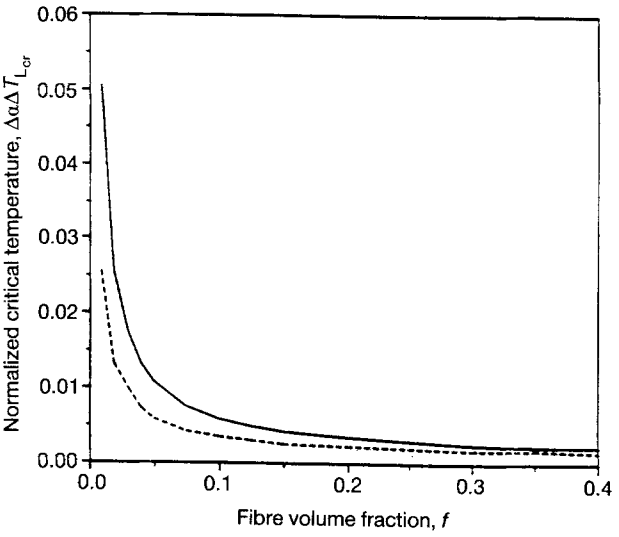

Figure 7 Normalized critical temperature change required to initiate uniform yielding of the matrix versus fibre volume fraction of a SiC/Al short-fibre composite with an aspect ratio of $\alpha = 4$. ——, $\beta = 0$; --- $\beta = \pi/2$ (2-D uniform distribution).

and cosine-type distributions, respectively. In the following discussion, the symbol $\boldsymbol{\sigma}$ is used to represent the volume averaged stress quantity and has the same meaning as $\langle\boldsymbol{\sigma}\rangle$. Both Figs 3 and 4 show that all three stress components increase with increasing volume fraction of fibre, f. It should also be noted that the dependence of $\boldsymbol{\sigma}$ on f is relatively linear up to $f \simeq 10\%$. Fig. 3 shows that an isotropic state of stress exists for a uniform distribution with $\beta = \pi/2$, i.e. $\sigma^{u}_{11} = \sigma^{u}_{22} = \sigma^{u}_{33}$, as shown by the solid line. This case corresponds to a completely random 3-D composite. For a cosine-type distribution at $\beta = \pi/2$, more fibres are aligned along the x_3-axis, thus the composite system is not isotropic and the axial stress (σ_{33}) is larger than the transverse stresses ($\sigma_{11} = \sigma_{22}$), as shown by the dashed curves. This is also the case in Fig. 4 and is true for any cut-off angle. Both Figs 3 and 4 show that for a given cut-off angle, in these cases $\pi/2$ and $\pi/3$, respectively, the fibre volume fraction has a much

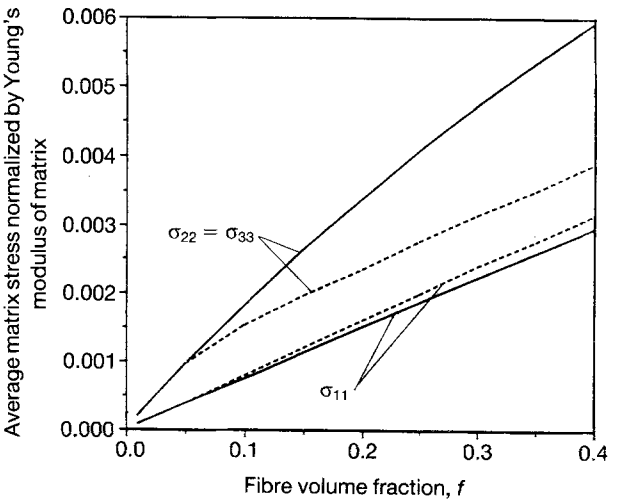

Figure 8 Variation of the normalized thermal residual stress in the matrix with the fibre volume fraction for 2-D in-plane misorientation with an elastic–plastic matrix. ——, σ^{E}; ---, σ^{EP}. $\alpha = 5$; $\beta = \pi/2$.

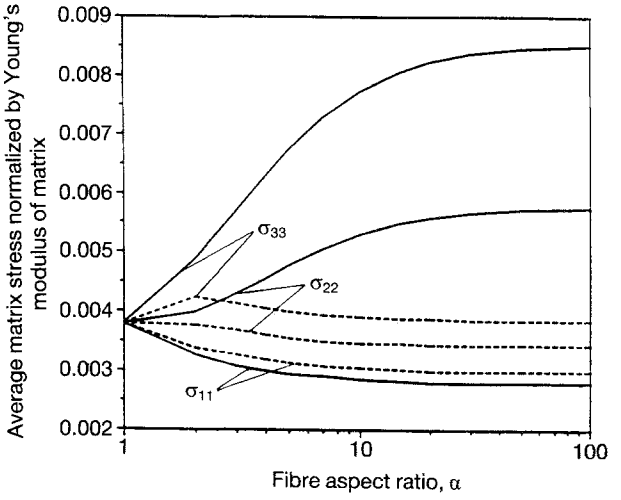

Figure 9 Normalized elastic (σ^{E}) and elastic–plastic (σ^{EP}) average stress in the matrix of a SiC/Al short-fibre composite as a function of the fibre aspect ratio. ——, σ^{E}; ---, σ^{EP}. $F = 0.4$; $\beta = \pi/3$, uniform distribution.

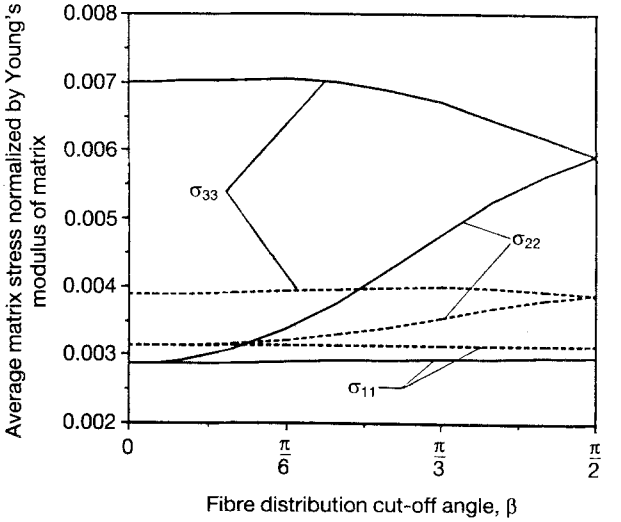

Figure 10 Variation of the normalized thermal residual stress in the matrix with the distribution cut-off angle for 2-D in-plane misorientation with an elastic–plastic matrix. ——, σ^{E}; ---, σ^{EP}. $f = 0.4$; $\alpha = 5$.

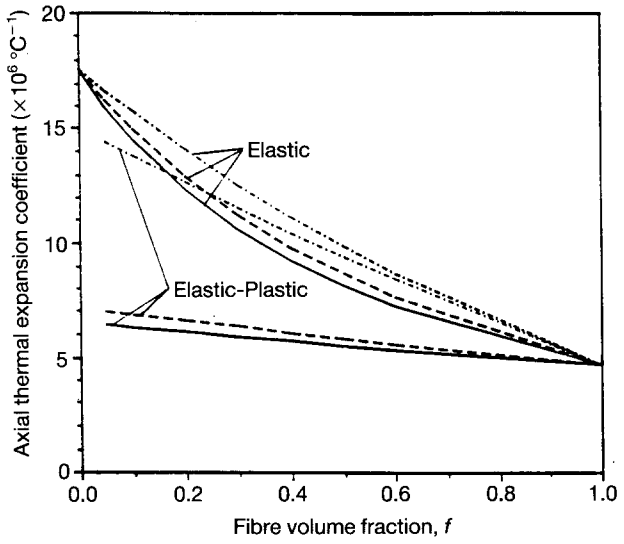

Figure 11 Axial thermal expansion coefficient versus fibre volume fraction for a tungsten/copper composite system ——, Aligned continuous fibre; - - -, aligned short fibre; . . . . . , 2-D random short fibre. $\alpha = 5$.

greater effect on all three stress components than the fibre orientation distribution *type*. The effect of fibre orientation distribution type, however, increases with increasing f. It should also be noted that as $f \to 0$, $\langle \boldsymbol{\sigma} \rangle_m \to 0$ which corresponds to a dilute suspension of fibres such that when averaged over the infinite domain, the disturbance stress in the matrix vanishes. The stresses in the fibre approach that obtained from Eshelby's solution [1] for a single inhomogeneity in an infinite elastic medium.

Fig. 5 shows the dependence of the average stress in the matrix normalized by Young's modulus of the matrix, $\langle \boldsymbol{\sigma} \rangle_m / E_m$, on the fibre-cut-off angle β where the aspect ratio ($\alpha = 5$) and fibre volume fraction ($f = 0.4$) are fixed. Again, both uniform (solid lines) and cosine-type (dashed lines) distributions are considered. At $\beta = \pi/2$ for a uniform distribution, all stress components coincide, i.e. $\sigma_{11}^u = \sigma_{22}^u = \sigma_{33}^u$, thus a completely isotropic composite, and for a cosine type distribution, $\sigma_{33}^c > \sigma_{11}^c = \sigma_{22}^c$, as explained in the preceding section. It is noted that $\sigma_{33}^u \approx \sigma_{33}^c$ and is approximately constant up to $\beta \approx \pi/6$. Over this span, however, $\sigma_{11} = \sigma_{22}$ does increase slightly. For the case where $\beta \to 0$, $\boldsymbol{\sigma}^u = \boldsymbol{\sigma}^c$ and these results coincide with the solution for an aligned short-fibre composite [10]. As Fig. 5 shows, the effect of fibre distribution type increases as the degree of fibre misorientation increases, i.e. as β increases. It can thus be concluded that an accurate assessment of the distribution type may not be necessary at lower values of the cut-off angle, and even that the simple solution for an aligned short-fibre composite may be acceptable for small degrees of misorientation. At larger values of β, however, it is apparent that both of these parameters significantly effect the thermal residual stress state and should be considered.

The effect of fibre aspect ratio, α, on the average matrix stress is shown in Fig. 6, where $\beta = \pi/3$ and $f = 0.4$. Fig. 6 shows that σ_{33} increases rapidly with α at low aspect ratios, but becomes saturated at $\alpha \simeq 30$. This phenomenon is observed with both uniform and cosine-type distributions, however, the cosine-type distribution tends to become saturated at slightly lower values of α. The other stress components, $\sigma_{11} = \sigma_{22}$, also increase more rapidly with α at lower values of α and become saturated at $\alpha \approx 30$. Here, though, $\sigma_{11}^c = \sigma_{22}^c$ is much less than $\sigma_{11}^u = \sigma_{22}^u$ as it becomes saturated. As $\alpha \to 1$ (spherical filler), all stress components for both types of distribution functions are equal and they coincide with the solution given by Taya *et al.* [5].

In Fig. 7, the normalized critical temperature change required to initiate uniform yielding of the matrix is studied for two 2-D SiC/Al MSFCs with distribution cut-off angles of $\beta = 0$ and $\beta = \pi/2$. These two cut-off angles correspond to an aligned short-fibre composite and a 2-D in-plane random short-fibre composite, respectively. These two cases thus bound $\Delta\alpha\Delta T_{cr}$ for all β, i.e. for all 2-D in-plane MSFCs, with all other parameters held constant. In Fig. 7, the difference between the two curves can be considered the variability in the range of completely elastic response (to the thermal loading) for a 2-D MSFC. It is seen that the effect of misoriented fibres (in-plane) increases the range of elastic response to thermal loading of the composite. This is of course at the expense of a decreased axial stiffness. It is seen, however, that the increased range of elastic response decreases rapidly with increasing fibre volume fraction. In fact at large volume fractions ($f \approx 0.5$) the effect of misoriented fibres on the range of elastic response is so small (≈ 31 °C) that it is probably insignificant for practical applications.

The normalized residual stresses for both the elastic and elastic–plastic models for a random 2-D in-plane MSFC ($\beta = \pi/2$, thus $\sigma_{22} = \sigma_{33} \neq \sigma_{11}$) are shown in Fig. 8. The in-plane stresses are affected much more than the out of plane stress. The yield condition of Equation 3.14 is seen to be satisfied after yield as the difference between the curves $\sigma_{22}^{EP} = \sigma_{33}^{EP}$ and σ_{11}^{EP} is constant and equal to the normalized yield strength of the matrix.

In Fig. 9, the effect of fibre geometry (aspect ratio) on the magnitude of elastic and elastic–plastic thermal residual stresses is investigated for a SiC/Al MSFC. Although after yielding the magnitude of the flow stress is constant, the magnitude of the hydrostatic stress is still important in some instances. For example in thermal stress finite element codes, the accuracy of a stress solution is a percentage of the magnitude of the total stress and can thus be very large when large hydrostatic stress components exist. At low aspect ratios, σ_{33}^E and σ_{33}^{EP} increase rapidly, but then remain approximately constant as the composite becomes saturated at $\alpha \approx 30$. At aspect ratios greater than $\alpha \approx 30$, the composite essentially behaves as one reinforced by continuous fibres ($\alpha \to \infty$). In both the elastic and elastic–plastic cases, σ_{11} and σ_{22} are less sensitive to α than σ_{33}. As $\alpha \to 1$, all stress components coincide and reduce to the result given by Taya *et al.* [3] for a particulate reinforced composite. In this case, relaxation due to uniform plastic flow of the matrix is energetically unfeasible, as the average matrix stress state is hydrostatic due to the isotropic

reinforcement. However, localized yielding will occur in reality and this is not accounted for in the present model.

Fig. 10 shows the normalized matrix stress versus the cut-off angle for a case when $\Delta\alpha\Delta T > \Delta\alpha\Delta T_{CR}$ for all β, i.e. the CTE mismatch is large enough to cause uniform yielding of the matrix for all β. Again, results for both the elastic (solid lines) and elastic–plastic (dashed lines) models are shown. It is seen that the relaxation due to plastic flow results in a decrease in σ_{33}^{EP} and an increase in σ_{11}^{EP} for all β relative to the elastic results. For this case, plastic flow results in an increase in σ_{22}^{EP} for the range of smaller β, then an increase in σ_{22}^{EP} for larger β (relative to the elastic results). This phenomenon is again a result of the requirement of volume constancy of the matrix. Fig. 10 also shows that $\sigma_{22} = \sigma_{33} \neq \sigma_{11}$ for $\beta = \pi/2$ (in-plane random MSFC) and $\sigma_{11} = \sigma_{22} \neq \sigma_{33}$ for $\beta = 0$ (aligned SFC). Note that the elastic–plastic model predicts that σ_{11}^{EP} and σ_{33}^{EP} are approximately constant over the entire range of β. However, as σ_{33}^{E} is not approximately constant over the range of β, the inelastic strain ε^{p} is also not approximately constant over the range of β. Thus, although the total residual stress predicted by the elastic–plastic model is nearly independent of β, the relaxation due to plastic flow that occurs to produce the final residual stress is dependent on β. It is important to recognize this fact in the case of a deformation analysis such as that of dimensional change of a composite due to thermal cycling.

Finally, with regard to the deformation of short-fibre composites, the axial thermal expansion coefficients (CTEs) of a 2-D W/Cu MSFC in both the elastic and elastic-plastic ranges are examined in Fig. 11. Three cases are considered: an aligned continuous fibre composite, an aligned short-fibre composite, and a 2-D in-plane random short-fibre composite. It is seen that the discontinuous reinforcement results in a composite that is more expansive as the large CTE of the matrix plays a more significant role. For both the aligned continuous and short-fibre composites, the elastic–pastic CTE is much smaller than the elastic CTE and can be approximated to the first order by the CTE of the fibre. This first order approximation can be formally obtained by neglecting the Poisson contraction of the composite in the transverse direction [27]. It is also evident from Fig. 11 that the effect of misoriented fibres on the axial CTE of the composite is much larger in the elastic–plastic range than in the elastic range. Fig. 11, however, does not completely describe the thermal expansion behaviour of 2-D MSFCs as expansions in the transverse and thickness directions, which are readily computed with the present model, must certainly be considered in practice. It should be noted that the result for the axial CTEs for the continuous fibre composite in Fig. 11 agrees with that of Wakashima *et al.* [19] which was derived by the minimization of free energy approach.

6. Conclusion

A micromechanics model has been proposed to analyse residual stresses and deformations that develop in short-fibre composites upon an applied uniform temperature change. The model is based on Eshelby's equivalent inclusion method and treats the interaction among fibres at finite volume fractions through the Mori–Tanaka mean field theory. The model treats the matrix as an elastic/plastic material while the fibre is elastic. The model is able to account for the effects of misoriented short fibres, the orientations of which are described by a density distribution function. Uniform and cosine-type distribution functions are used to simulate actual distributions of misoriented fibres. Based on the numerical results above, it is seen that the misorientation of short fibres has a significant effect on both the stress and deformation behaviour of short-fibre composites. Misoriented short fibres can increase the range of thermoelastic response of a short fibre composite; however, this is at the expense of a reduced elastic stiffness.

References

1. J. D. ESHELBY, *Proc. R. Soc. (Lond.)* **A241** (1957) 376.
2. T. MORI and K. TANAKA, *Acta Metall.* **21** (1973) 571.
3. V. M. LEVIN, *Mekhanika Tverdogo Tela* (1967) 88.
4. B. W. ROSEN and Z. HASHIN, *Int. J. Engng Sci.* **8** (1970) 157.
5. M. TAYA, S. HAYASHI, A. S. KOBAYASHI and H. S. YOON, *J. Amer. Cer. Soc.* **73** (1990) 1382.
6. H. M. LEDBETTER and M. W. AUSTIN, *Mater. Sci. Engng* **89** (1987) 53.
7. M. ORTIZ and A. MOLINARI, *J. Mech. Phys. Solids* **36** (1988) 385.
8. R. M. CHRISTENSEN and K. H. LO, *ibid.* **27** (1979) 315.
9. Y. MIKATA and K. TAYA, *J. Comp. Mater.* **19** (1985) 554.
10. R. J. ARSENAULT and M. TAYA, *Acta Metall.* **35** (1987) 651.
11. M. TAYA and R. J. ARSENAULT, "Metal Matrix Composites, Thermomechanical Behavior" (Pergamon, Oxford, 1989). Ch. 3.
12. P. J. WITHERS, D. J. JENSEN, H. LILHOLT and W. M. STOBBS, in "Proceedings of the ICCM-6/ECCM-2", edited by F. L. Matthews, N. C. R. Buskell, J. M. Hodgkinson and J. Morton (Elsevier, North-Holland, 1987) p. 2.255.
13. M. TAYA, M. DUNN, B. DERBY and J. WALKER, *Appl. Mech. Rev.* **43** (1990) S294.
14. Y. TAKAO, in "Recent Advances in Composites in the United States and Japan", edited by J. R. Umson and M. Taya, ASTM STP 864 (American Society for Testing and Materials, Philadelphia, 1985) p. 685.
15. Y. TAKAO and M. TAYA, *J. Appl. Mech.* **107** (1985) 806.
16. G. P. TANDON and G. J. WENG, *ibid.* **55** (1988) 126.
17. G. J. DVORAK, *ibid.* **53** (1986) 737.
18. K. TANAKA, K. WAKASHIMA and T. MORI, *J. Mech. Phys. Solids* **21** (1973) 207.
19. K. WAKASHIMA, M. OTSUKA and S. UMEKAWA, *J. Comp. Mater.* **8** (1974) 391.
20. Y. P. QUI and G. J. WENG, *Int. J. Engng Sci.* **28** (1990) 1121.
21. P. J. WITHERS, *Phil Mag. A* **59** (1989) 759.
22. T. MURA, "Micromechanics of Defects in Solids", 2nd edn. (Martinus Nijhoff, Dordrecht, 1987).
23. M. TAYA and T. MORI, in "Thermomechanical Couplings in Solids", edited by H. D. Bui and Q. S. Nguyen (Elsevier, North-Holland, 1987) p. 147.
24. P. J. WITHERS, W. M. STOBBS and O. B. PEDERSEN, *Acta Metall.* **37** (1989) 3061.
25. T. J. WARNER and W. M. STOBBS, *ibid.* **37** (1989) 2873.
26. O. B. PEDERSEN and L. W. BROWN, *ibid.* **25** (1977) 1303.
27. O. B. PEDERSEN, in "Micromechanics and Inhomogeneity", Toshio Mura Anniversary Volume, edited by G. J. Weng, M. Taya and H. Abe, (Springer–Verlag, New York 1987) p. 341.

Received 23 September 1992
and accepted 21 September 1993

Appendix ψ^i and P and Q matrices

For 2-D in-plane misorientation ψ^i, P, and Q are given by Taya *et al.* [13]. For 3-D axisymmetric misorientation, ψ^i are given by:

$$\psi^u = 1 - \cos\beta$$

$$\psi^c = \frac{1}{2}\left[\frac{\cos(a-1)\beta - 1}{a-1} - \frac{\cos(a+1)\beta - 1}{a+1}\right] \quad \text{(A1)}$$

The explicit forms of the non-zero elements of P and Q for both uniform and cosine-type density distribution functions are:

$$\begin{aligned}
P_{11} &= \tfrac{3}{8}[A_{11}(C_0+C_4)+A_{33}S_4+(A_{13}+A_{31})C_5 \\
&\quad + \tfrac{1}{2}A_{44}S_3] + \tfrac{1}{8}[(2A_{12}+2A_{66})C_2 \\
&\quad + (A_{13}+A_{31}+2A_{44})S_2] \\
P_{12} &= \tfrac{1}{8}[A_{11}(C_0+C_4)+A_{33}S_4+(A_{13}+A_{31})C_5 \\
&\quad + \tfrac{1}{2}A_{44}S_3] + \tfrac{3}{8}[(2A_{12}-\tfrac{2}{3}A_{66})C_2 \\
&\quad + (A_{13}+A_{31}-\tfrac{2}{3}A_{44})S_2] \\
P_{13} &= \tfrac{1}{2}[A_{13}(C_2+C_4)+A_{31}S_4+A_{12}S_2 \\
&\quad + (A_{11}+A_{33})C_5 - \tfrac{1}{2}A_{44}S_3] \\
P_{31} &= \tfrac{1}{2}[A_{31}(C_2+C_4)+A_{13}S_4+A_{12}S_2 \\
&\quad + (A_{11}+A_{33})C_5 - \tfrac{1}{2}A_{44}S_3] \\
P_{33} &= A_{11}S_4 + A_{33}C_4 + (A_{13}+A_{31})C_5 + \tfrac{1}{2}A_{44}S_3 \\
P_{44} &= \tfrac{1}{2}[A_{44}(C_2+C_3)+A_{66}S_2 \\
&\quad + \tfrac{1}{2}(A_{11}-A_{13}-A_{31}+A_{33})S_3] \\
P_{66} &= \tfrac{1}{2}[P_{11}-P_{12}] \qquad \text{(A2)}
\end{aligned}$$

and

$$\begin{aligned}
Q_{11} &= \tfrac{1}{2}C_2 \\
Q_{12} &= \tfrac{1}{2}C_0 \\
Q_{13} &= \tfrac{1}{2}S_2 \\
Q_{15} &= \tfrac{1}{2}S_5 \\
Q_{31} &= S_2 \\
Q_{33} &= C_2 \\
Q_{35} &= -S_5 \qquad \text{(A3)}
\end{aligned}$$

where A_{ij} is defined in Equation 3.7 and the symmetry of A_{ij} has been used. The S_i and C_i items are dependent on the fibre distribution function and cut-off angle. For a uniform distribution, they are given by:

$$C_0 = 1 - \cos\beta$$

$$C_2 = \frac{1-\cos^3\beta}{3}$$

$$C_3 = \frac{1}{2}\left[-\cos\beta + \frac{\cos^3\beta}{6} - \frac{\cos^5\beta}{10} + \frac{14}{15}\right]$$

$$C_4 = \frac{1-\cos^5\beta}{5}$$

$$C_5 = \frac{\cos\beta}{5}\left[\sin^4\beta - \frac{\sin^2\beta}{3} - \frac{2}{3} + \frac{2}{3\cos\beta}\right]$$

$$S_2 = -\frac{1}{12}[9\cos\beta - \cos^3\beta - 8]$$

$$S_3 = \frac{1}{2}\left[-\cos\beta - \frac{\cos^3\beta}{6} + \frac{\cos^5\beta}{10} + \frac{16}{15}\right]$$

$$S_4 = \frac{\cos\beta}{5}\left[-\sin^4\beta - \frac{4\sin^2\beta}{3} - \frac{8}{3} + \frac{8}{3\cos\beta}\right]$$

$$S_5 = \frac{1}{2}\left[\sin\beta - \frac{\sin 3\beta}{3}\right] \qquad \text{(A4)}$$

For a cosine-type distribution, C_i and S_i are given by:

$$\begin{aligned}
C_0 &= \tfrac{1}{2}E_1 \\
C_2 &= \tfrac{1}{8}[E_1 + E_3] \\
C_3 &= \tfrac{1}{4}[E_1 - \tfrac{1}{2}E_3 + \tfrac{1}{2}E_5] \\
C_4 &= \tfrac{1}{16}[E_1 + \tfrac{3}{2}E_3 + \tfrac{1}{2}E_5] \\
C_5 &= \tfrac{1}{16}[E_1 + \tfrac{1}{2}E_3 + \tfrac{1}{2}E_5] \\
S_2 &= \tfrac{1}{8}[3E_1 - E_3] \\
S_3 &= \tfrac{1}{4}[E_1 + \tfrac{1}{2}E_3 - \tfrac{1}{2}E_5] \\
S_4 &= \tfrac{1}{16}[5E_1 - \tfrac{5}{2}E_3 + \tfrac{1}{2}E_5] \\
S_5 &= \tfrac{1}{4}[E_7 - E_9] \qquad \text{(A5)}
\end{aligned}$$

where:

$$E_1 = \frac{\cos(a-1)\beta - 1}{a-1} - \frac{\cos(a+1)\beta - 1}{a+1}$$

$$E_3 = \frac{\cos(a-3)\beta - 1}{a-3} - \frac{\cos(a+3)\beta - 1}{a+3}$$

$$E_5 = \frac{\cos(a-5)\beta - 1}{a-5} - \frac{\cos(a+5)\beta - 1}{a+5}$$

$$E_7 = \frac{\sin(a-1)\beta}{a-1} + \frac{\sin(a+1)\beta}{a+1}$$

$$E_9 = \frac{\sin(a-3)\beta}{a-3} + \frac{\sin(a+3)\beta}{a+3} \qquad \text{(A6)}$$

where β is the cut-off angle.